Controlling spin ordering in frustrated magnets via thin film heteroepitaxy

Jodi M. Iwata-Harms, Franklin J. Wong, Urusa S. Alaan, B. J. Kirby, Julie A. Borchers, Michael F. Toney, Brittany B. Nelson-Cheeseman, Marco Liberati, Elke Arenholz, and Yuri Suzuki

Phys. Rev. B **85**, 214424 — Published 20 June 2012

DOI: 10.1103/PhysRevB.85.214424

Controlling spin ordering in frustrated magnets via thin film heteroepitaxy

Jodi M. Iwata-Harms,[1] Franklin J. Wong,[1,2] Urusa S. Alaan,[1] B. J. Kirby,[3] Julie A. Borchers,[3] Michael F. Toney,[4] Brittany B. Nelson-Cheeseman,[1] Marco Liberati,[5] Elke Arenholz,[5] and Yuri Suzuki[1,2,6]

[1]*Department of Materials Science and Engineering, University of California, Berkeley, CA 94720, USA*
[2]*Materials Sciences Division, Lawrence Berkeley National Laboratory, Berkeley, CA 94720, USA*
[3]*NIST Center for Neutron Research, National Institute of Standards and Technology, Gaithersburg, MD 20899, USA*
[4]*Stanford Synchrotron Radiation Lightsource, SLAC National Accelerator Laboratory, Menlo Park, CA 94025, USA*
[5]*Advanced Light Source, Lawrence Berkeley National Laboratory, Berkeley, CA 94720, USA*
[6]*Department of Applied Physics and Geballe Laboratory for Advanced Materials, Stanford University, Stanford, CA 94305, USA*

(Dated: April 5, 2012)

Competing exchange interactions can give rise to varying degrees of frustration that manifest itself in non-collinear magnetic moment ordering or canonical geometric frustration in magnets with large ground state degeneracies. Relieving this frustration has the potential to stabilize ground states inaccessible in the bulk. We demonstrate that heteroepitaxial lattice distortions can modify the strength of exchange interactions in thin films of the frustrated ferrimagnet, $CuCr_2O_4$. The reduction of magnetic frustration in $CuCr_2O_4$ through lattice distortions results in greater collinear spin ordering in $CuCr_2O_4$ thin films and an enhanced magnetization. We identify heteroepitaxial lattice distortions as a method to tune spin functionality and potentially lift ground state degeneracies more broadly in frustrated magnets.

PACS numbers: 75.25.-j,75.50.Gg,75.30.Et,75.70.Ak

Magnets with varying degrees of frustration can give rise to non-collinear magnetic ordering or canonical geometric frustration characterized by large ground state degeneracies. The properties of these frustrated systems are particularly susceptible to small perturbations such as electric and magnetic fields, chemical modification, and strain. With advances in thin film deposition techniques, we can use heteroepitaxy to explore new spin phase space regions in these frustrated magnets. Of particular interest are spinel structure compounds with magnetic cations. The chromite spinels (ACr_2O_4) display magnetic ground states that range from highly frustrated systems like canonical geometrically frustrated magnets[1] to those with reduced frustation such as non-collinear spin systems that exhibit helicoidal[2–4] and triangular, canted[5,6] order. Theoretical studies have focused on their spin ordering stability,[7] and experimental studies have uncovered spin-lattice coupling,[8] multiferroicity,[9–11] and magnetism-induced anisotropic lattice dynamics.[12] In heterostructures, the chromites have revealed large junction magnetoresistance and spin filtering demonstrating their potential for oxide-based spintronics.[13–15] The ability to tune the physical properties of spinel chromites is the first step towards exploiting new ground states in canted and strongly geometrically frustrated magnetic oxides.

There have been numerous studies for which heteroepitaxial strain has given rise to emergent phenomena or tuned functionality in complex oxides.[16,17] In many of these studies, heteroepitaxial strain induces lattice distortions that, in turn, modify the electronic structure and magnetic ordering.[18] However epitaxial strain may lift the degeneracy of the ground states of frustrated magnets through the modification of exchange interactions, thus providing a different approach for controlling spin order in oxide thin films. A model system for the study of such effects is the tetragonal, canted ferrimagnet, $CuCr_2O_4$ (CCO). $CuCr_2O_4$ exhibits non-collinear moment ordering due to the presence of closely competing exchange interactions between magnetic moments of the tetrahedrally and octahedrally coordinated cations.

In this work, we demonstrate the lifting of magnetic frustration through the modification of exchange interactions with heteroepitaxy. More specifically we demonstrate that by decreasing the tetragonality of the CCO unit cell and thus yielding greater collinear alignment between the Cr^{3+} moments, we heal the frustration of the magnetic moments in CCO thin films and significantly enhance the magnetization compared to that of bulk. X-ray diffraction (XRD) indicates that epitaxial strain stabilizes a more cubic unit cell compared to the bulk in isostructural CCO films on $MgAl_2O_4$ (MAO) substrates. Bulk magnetometry measurements performed with a superconducting quantum interference device (SQUID) magnetometer demonstrate enhanced magnetization. Neutron reflectivity (NR) shows magnetic uniformity in the films, thus eliminating surface or interface effects as the source of enhancement. Element-specific X-ray magnetic circular dichroism (XMCD) studies suggest that the increased net moment of Cr^{3+} is responsible for the enhanced magnetization.

Bulk CCO is an insulating ferrimagnetic spinel oxide with a tetragonal unit cell (a = 6.03 Å, c = 7.78 Å) and c/a ratio of 1.29 (Fig. 1).[5] Its body-centered tetragonal lattice is formed by Cu^{2+} (1 μ_B) cations which occupy the tetrahedral sites because the Cr^{3+} (3 μ_B) cations strongly prefer the octahedral sites.[5,19] The edge-shared Cr^{3+} octahedral cages result in a geometrically

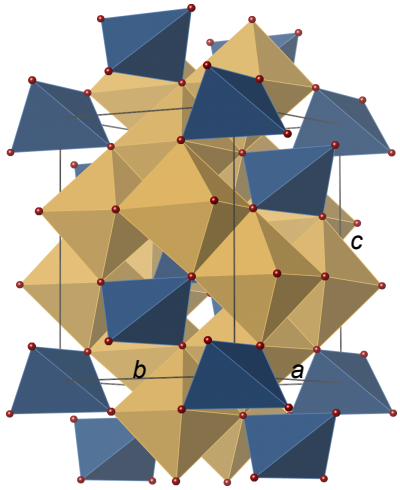

FIG. 1. (Color online) Schematic of the $CuCr_2O_4$ spinel structure showing the edge-sharing Cr^{3+} octahedra (yellow) formed by oxygen anions (red, size reduced for clarity); the Cr^{3+} octahedra are corner shared with the Cu^{2+} tetrahedra (blue).

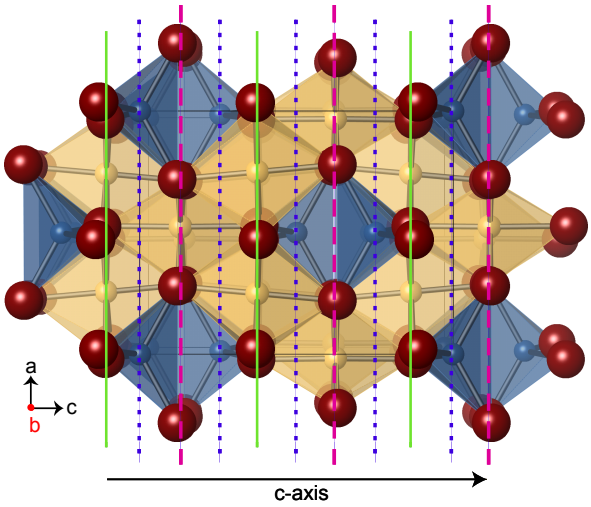

FIG. 2. (Color online) The [010] projection of the crystal structure. Solid (lime) and dashed (magenta) lines highlight alternating (004) planes containing Cr and blue (dotted) lines represent (008) Cu planes. Within each (008) plane, the moments of the intraplanar cations are aligned parallel to each other in the ab-plane; however, between nearest neighbor (004) Cr^{3+} planes, the moments are canted with respect to each other. The Cu^{2+} moments are aligned antiparallel to the net Cr^{3+} moment. In CCO thin films, heteroepitaxy increases the distance between these planes along the c-axis.

frustrated lattice as the antiferromagnetic exchange interactions among nearest neighbor Cr^{3+} cations cannot be simultaneously satisfied with Ising spins.[1] This leads to a large macroscopic ground state degeneracy in the presence of structural order.[1] However, the tetragonal distortion induced by the presence of magnetic, Jahn-Teller active $3d^9$ Cu^{2+} in the tetrahedral sites removes this degeneracy favoring an ordered state with strong competing exchange interactions in which the exchange energy between Cu^{2+} and Cr^{3+}, $H_{Cu2+-Cr3+}$, is on the order of $H_{Cr3+-Cr3+}$ using the classical Heisenberg model.[20] This results in a compressed c-axis with respect to a face-centered tetragonal reference, and triangular, canted Yafet-Kittel magnetic ordering.[5,20,21] As discussed in Fig. 2, moments within the (004) planes exhibit long-range, parallel alignment; however, the Cr^{3+} moments between adjacent (004) planes are canted relative to each other by the angle $\varphi_{bulk} = 151°$.[5] This results in a low magnetic moment of 0.51 μ_B f.u.$^{-1}$ which is an order of magnitude smaller than 5 μ_B f.u.$^{-1}$ of the Neél configuration.[5]

CCO thin films were grown by pulsed laser deposition on cubic (110) spinel MAO (a = 8.08 Å) and perovskite $SrTiO_3$ (STO) (a = 3.905 Å) substrates. The films were grown at 500 °C in 15 mTorr of O_2 with a KrF laser and fluence of approximately 1 J cm^{-2}. The structure of our films was characterized with four-circle XRD at 8000 eV on beamline 7-2 at the Stanford Synchrotron Radiation Lightsource (SSRL) and by cross-sectional high-resolution transmission electron microscopy (HRTEM) using a Philips CM300FEG microscope at the National Center for Electron Microscopy at Lawrence Berkeley National Laboratory (LBNL). Element-specific cation valence information was obtained from *L*-edge X-ray absorption (XA) spectroscopy on beamlines 6.3.1 and 4.0.2 of the Advanced Light Source (ALS). Site-specific elemental information was obtained from resonant X-ray scattering (RXS) measurements on beamlines 7-2 and 2-1 at SSRL. Film thicknesses were determined by Rutherford backscattering spectroscopy (RBS) at the Ion Beam Analysis Facility at LBNL and confirmed by X-ray reflectivity (XRR) on a Philips Analytical X'pert MRD diffractometer.

The bulk magnetization of the CCO films was measured in a Quantum Design MPMS 5XL SQUID magnetometer. The magnetic depth profile was extracted from NR measurements performed at the NIST Center for Neutron Research on the NG-1 reflectometer. For polarized neutron reflectivity (PNR), CCO samples were field cooled at 1.5 T to 5 K and measured at 660 mT. Unpolarized NR was performed at 7 T. Both PNR and NR used the specular reflectivity geometry. Element-specific magnetic XMCD measurents were performed at 25 K in total electron yield mode at normal incidence at beamlines 6.3.1 and 4.0.2 of the ALS.

RBS confirmed the 1:2 ratio of Cu to Cr cations, to within 5% standard error of the measurement, for our CCO films. The Cr *L*-edge XA spectra were consistent with octahedrally-coordinated Cr^{3+} while the Cu *L*-edge XA spectra were indicative of Cu^{2+}.[22,23] To identify the coordination of Cu, we use RXS.[24] In general, for a cubic spinel, the structure factor of the 220 reflection is dependent only on the tetrahedral sites. For the 220 reflection of CCO (Fig. 3), we observe a strong decrease

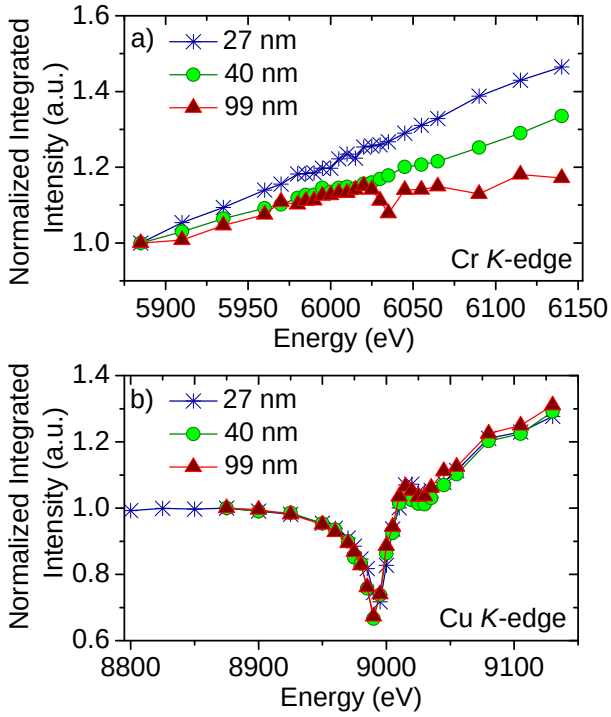

FIG. 3. (Color online) RXS of the 220 reflection of CCO films with varying thickness at the (a) Cr and (b) Cu K-edge.

in the diffracted peak intensity due to absorption at the Cu K-edge. This indicates that the 220 planes are occupied by Cu with tetrahedral coordination. A nominal decrease in the 220 diffracted peak intensity at the Cr K-edge suggests a small amount, if any, of tetrahedral Cr consistent with bulk studies.[19] These studies indicate that the bulk valence states and site occupancies are robust and preserved in the thin films, thereby eliminating cation inversion and changing valence states as sources of the enhanced magnetization.

We grew a series of CCO thin films ranging in thickness from 7 to 148 nm. To facilitate epitaxial growth, we selected (110) MAO and (110) STO substrates that provide a rectangular surface unit cell to tetragonal CCO. For MAO substrates, the lattice mismatch along substrate edge directions are +3.8% along [001]CCO||[001]MAO, and -5.8% along [010]CCO||[1$\bar{1}$0]MAO. For STO substrates, the lattice mismatch along substrate edge directions are +0.39% along [001]CCO||[001]STO, and -8.72% along [010]CCO||[1$\bar{1}$0]STO. While the mismatch along the [001] direction is significantly smaller for samples on STO compared to MAO, the mismatch along the [010]CCO direction is substantially larger for samples on STO.

HRTEM and its Fourier transform of CCO films on MAO and STO are shown in Fig. 4. CCO films on MAO exhibit isostructural growth; whereas CCO films on STO exhibit regions with defective stacking of the {111} planes with respect to the substrate crystal. XRD

FIG. 4. Cross-sectional HRTEM image and Fourier transform (substrate directions are shown) recorded along the [010]CCO||[1$\bar{1}$0] substrate zone axis for (a) MAO and (b) STO. CCO films on MAO substrates show isostructural growth; whereas CCO films on STO substrates exhibit regions with defective stacking of the {111} planes with respect to the substrate crystal.

TABLE I. Lattice parameters of CCO films on MAO of varying thickness as determined by XRD.

Film Thickness (nm)	a (Å)	b (Å)	c (Å)	c/a
7	5.93	5.87	8.19	1.38
27	5.93	5.94	7.95	1.34
57	5.95	5.96	7.915	1.33
71	5.95	5.96	7.89	1.325
99	5.95	5.98	7.84	1.32
BULK	6.03	6.03	7.78	1.29

of CCO films on STO exhibited similar film diffraction peak positions regardless of thickness, thus suggesting that all CCO films on STO are more or less relaxed. For these reasons, we focus on the properties of CCO on MAO. We find that CCO on MAO grows epitaxially with rocking curve full-width half maxima ranging between 0.07° to 0.27°. By probing the 400, 040, and 202 reflections, we observed systematic shifts of the CCO diffraction peaks towards bulk with increasing film thickness. These reflections also determined both the in-plane and the out-of-plane lattice parameters of the CCO films. In Table I we see that the lattice parameters become more bulk-like for thicker films. The c/a ratio indicates reduced tetragonality for thinner films with the c/a ratio moving towards the cubic value of $\sqrt{2}$.[25] Strain calculations show that the tensile strain along [001]CCO ranges from 0.8% to 5.3% with decreasing film thickness, and is greater than the compressive strain along [010]CCO which ranges from about -0.8% to -2.6%.

The more cubic unit cell of CCO thin films has strong implications on their magnetic properties due to the strong coupling between structure and magnetism. Using RBS to determine the thickness of two 99 nm CCO films grown simultaneously on STO and MAO, we find

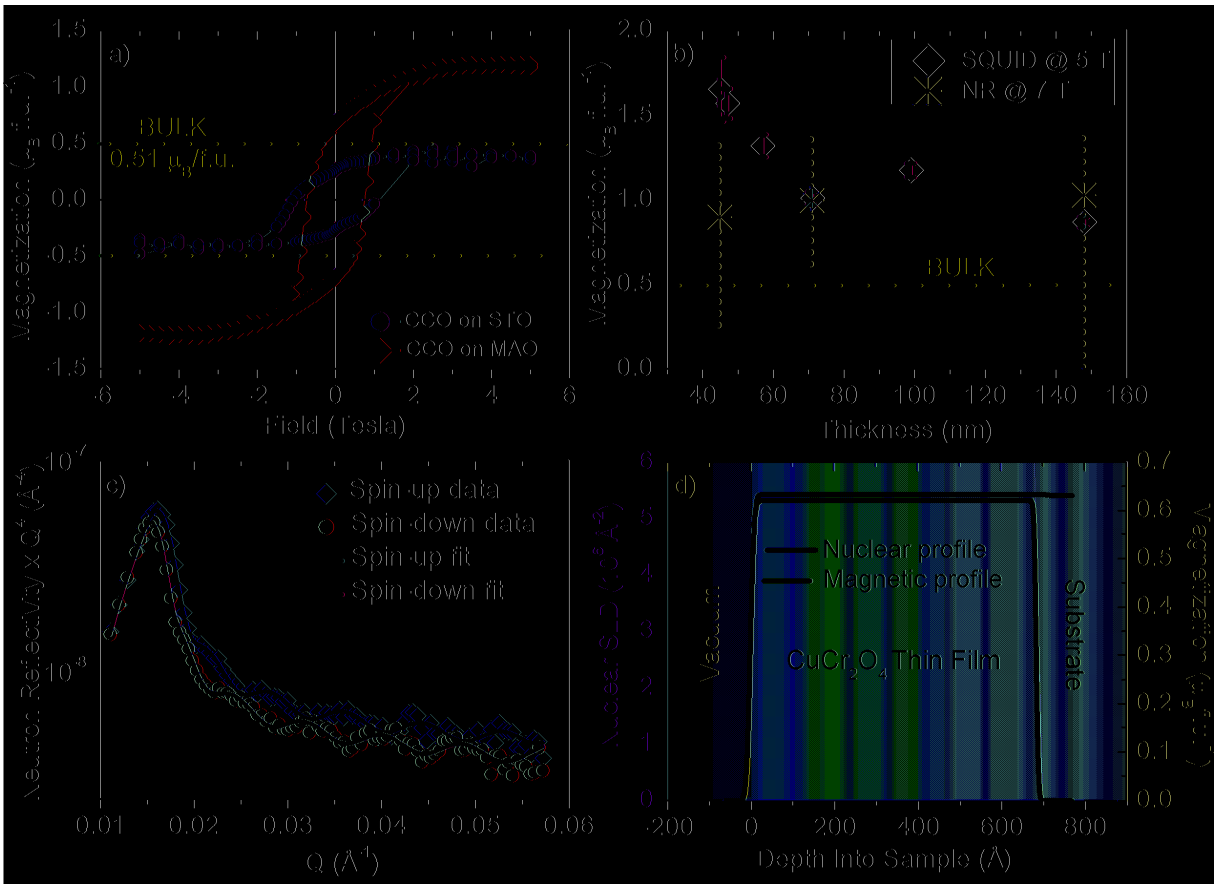

FIG. 5. (Color online)(a) Hysteresis loops for 99 nm CCO films grown on STO and MAO substrates obtained by SQUID magnetometry with an applied field along the out-of-plane [100]CCO direction. (b) M_s values for CCO films on MAO substrates of varying thickness at 5 K obtained from SQUID magnetometry and NR when measured along the in-plane [010]CCO direction. (c) PNR spectra of the spin-up and spin-down channels for a 71 nm film fitted to model the magnetic and nuclear profiles of the sample at 660 mT (unsaturated). (d) Model created to fit PNR spectra gives the depth profiles of the nuclear SLD (red line) and magnetization (blue line). The magnetic depth profile indicates uniform magnetization throughout the depth of the film.

that the hysteresis loops of these films at 5 K in Fig. 5 (a) demonstrate differences in saturation magnetization (M_s) when measured with SQUID magnetometry along the out-of-plane [100]CCO. CCO on STO has a nearly bulk-like magnetization value which is attributed to lattice relaxation due to the large lattice mismatch along the [010]CCO direction; whereas CCO on MAO exhibits a dramatically enhanced M_s exceeding that of bulk. Fig. 5 (b) shows a general trend of higher magnetization in thinner films of CCO on MAO in which M_s values up to 1.7 μ_B f.u.$^{-1}$ are obtained when measured along the [010]CCO direction. Since CCO films have a (001) magnetically easy plane and magnetocrystalline anisotropy effects are dominant, magnetic properties measured along out-of-plane [100]CCO and in-plane [010]CCO are considered equivalent.[25]

PNR was used to probe the depth profile of CCO films as it is directly sensitive to the layer magnetization and nuclear composition.[26–28] In Fig. 5 (c), the spin-up and spin-down non-spin flip scattering for a 71 nm film is measured with a 660 mT field applied along [010]CCO at 5 K. These spectra are sensitive only to the in-plane component of magnetization. The structure and the distinct oscillations are indicative of characteristic scattering lengths. From known isotopic scattering lengths[29] that predict the absence of nuclear contrast and experimental verification that reveal a damped signal, we can conclude that the oscillations are due to magnetic contrast. Spin-flip scattering, which originates from a net in-plane magnetization perpendicular to the field, is absent, thus indicating a (001) magnetically easy plane. Using exact dynamical formalism,[27] we modeled the PNR data to obtain the nuclear scattering length density (SLD) and magnetization profiles of the CCO samples. Fig. 5 (d) shows that the PNR data are consistent with a uniform magnetization throughout the depth of the film.[30] The absence of any inhomogeneity in the magnetic profile indicates that the enhancement is due to neither interfacial nor surface effects.

To extract M_s, we performed scattering measurements

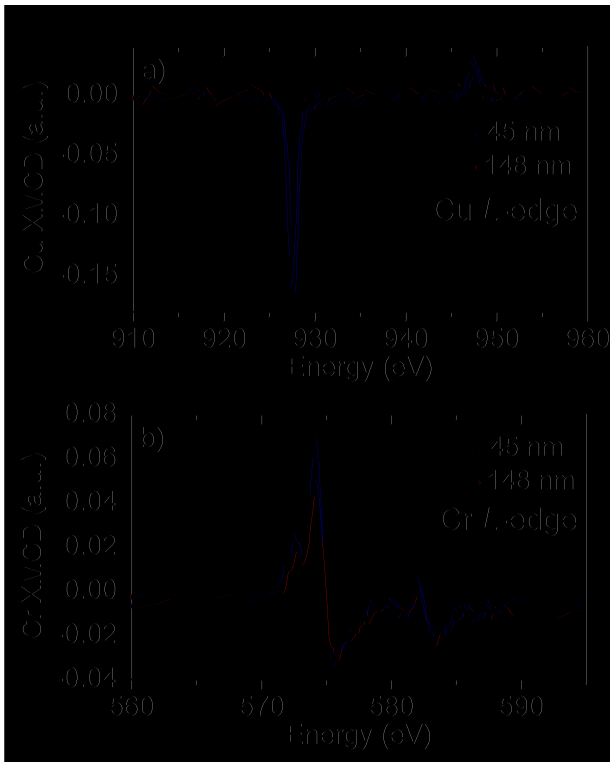

FIG. 6. (Color online) (a) Cu and (b) Cr L-edge XMCD at 25 K measured along [100]CCO.

at 5 K in higher fields with an unpolarized neutron beam to avoid difficulties in maintaining neutron spin orientation at high fields. As in the PNR data, any oscillation observed with unpolarized neutron reflectometry (NR) is purely magnetic in origin, thus allowing for the calculation of M_s when measured in a 7 T field. A direct comparison (Fig. 5 (b)) of the M_s values extracted from NR and SQUID magnetometry show that the magnetization is enhanced compared to that of bulk. For the 71 and 148 nm films, PNR corroborates the approximately two-fold increase in M_s observed by SQUID. However, for the thinner 45 nm film, SQUID magnetometry indicates that the magnetization increases to nearly 1.7 μ_B f.u.$^{-1}$ while NR finds that the magnetization decreases to 0.90 μ_B f.u.$^{-1}$ This discrepancy is attributed to error associated with our methods for extracting the magnetization of the film in SQUID magnetometry; in particular, removal of the diamagnetic contribution from the MAO substrates and imperfect sample shapes.

Finally, XMCD studies were performed to investigate element-specific magnetization. Fig. 6 shows the Cu and Cr L-edge XMCD spectra, normalized to the incoming photon flux, for 45 and 148 nm thick CCO samples in an applied field of $\pm$1.8 T. The anti-parallel orientation of the Cu and Cr XMCD spectra is consistent with ferrimagnetic alignment in which the net Cr moment is parallel to the applied field. The XMCD peak intensities for the Cu^{2+} and Cr^{3+} edges of the two films inform us about the origin of the changing magnetization observed in bulk measurements. According to SQUID magnetometry, the magnetization of the 45 nm film was 80-90% higher than the 148 nm film. In Fig. 6 (a), the Cu XMCD signal of the 45 and 148 nm films are essentially the same. However, in Fig. 6 (b) the peak Cr^{3+} dichroism signal changes approximately 30%. The discrepancy in the magnitude of the increased magnetization between the two techniques is attributed to the low 1.8 T field that is inadequate for magnetic saturation in the XMCD measurements. Thus, the increased signal from the Cr^{3+} cations and the net Cr moment aligned parallel to the field indicate that increased magnetization of the thinner films can be attributed to more collinear moment alignment of Cr^{3+} between adjacent (004) planes.

In bulk CCO, the tetragonal structure and triangular ground state moment configuration are the result of competition between the exchange and Jahn-Teller energies. The reduced symmetry results in longer intraplanar Cr-O bonds on the (004) planes and shorter interplanar Cr-O bonds orthogonal to the plane along the c-axis. This modification introduces two new exchange terms, $J'_{Cu2+-Cr3+}$ and $J'_{Cr3+-Cr3+}$ to account for the distorted c-axis. Kaplan *et al.* used four dominant exchange interaction terms ($J_{Cu2+-Cu2+}$ is small due to proximity and thus neglected): $J_{Cu2+-Cr3+}$, $J'_{Cu2+-Cr3+}$, $J_{Cr3+-Cr3+}$, and $J'_{Cr3+-Cr3+}$ rather than two to express the magnetic coupling between the cations because $J_{Cu2+-Cr3+} \neq J'_{Cu2+-Cr3+}$ and $J_{Cr3+-Cr3+} \neq J'_{Cr3+-Cr3+}$.[7] Here $J_{Cr3+-Cr3+}$ represents the exchange coupling between Cr^{3+} cations within the same ab-plane, and $J'_{Cr3+-Cr3+}$ describes the Cr^{3+}-Cr^{3+} coupling between Cr^{3+} cations on different ab-planes along the c-axis. $J_{Cu2+-Cr3+}$ represents Cu-O-Cr superexchange coupling via Cr-O bonds within an ab-plane, and $J'_{Cu2+-Cr3+}$ represents Cu-O-Cr superexchange coupling via Cr-O bonds between the ab-planes. In CCO films, lattice distortions induced by substrate strain modify the strength of these exchange interactions leading to enhanced magnetization. The exchange interactions are governed by nearest neighbor interactions which include an approximately 125° antiferromagnetic superexchange between Cu^{2+} - Cr^{3+}, 90° ferromagnetic superexchange between Cr^{3+} - Cr^{3+}, and antiferromagnetic direct exchange between the Cr^{3+} - Cr^{3+}.[31] The largest induced lattice distortion arising from epitaxy is the elongation of the c-axis, as shown in Table I, which increases the symmetry of CCO by stabilizing a more cubic unit cell and reduces the degree of direct overlap between Cr^{3+} orbitals on (220) and (2$\bar{2}$0) planes.

Our results demonstrate a route for using heteroepitaxy to stabilize greater magnetic ordering in canted magnetic systems. To account for the magnetic enhancement in our epitaxial CCO films, we propose that lattice distortions induced by epitaxial strain reduce the frustration thereby allowing for the rotation of the Cr^{3+} moments towards a more collinear alignment. The degree of moment rotation for Cr^{3+}, represented by φ, can be estimated from SQUID magnetometry data as-

suming negligible out-of-plane moment rotations. While octahedra rotations are possible, their effects are difficult to quantify with the characterization techniques used. (PNR cannot rule out the presence of tilting of the magnetization away from the field direction). The magnetization values in Fig. 5 (b) are consistent with ferrimagnetic alignment between Cr^{3+} and Cu^{2+} with φ ranging between 121° - 142° compared to the bulk value of 151°. For tetragonal CCO, Kaplan has shown that the angle of canting is related to the ratio of three exchange terms in which $cos(\frac{\varphi}{2}) = (2J_{Cu2+-Cr3+} + J'_{Cu2+-Cr3+})/(4J'_{Cr3+-Cr3+})$.[32] As φ is lower in thin films than in bulk, the strength of the exchange interactions in CCO must be affected by lattice distortions induced by heteroepitaxy. The reduction in interaction strength between interplanar Cr^{3+} predominantly affects the associated exchange terms, $J'_{Cu2+-Cr3+}$ and $J'_{Cr3+-Cr3+}$. Concomitant with the modified orbital overlap, we believe the decreased $J'_{Cr3+-Cr3+}$ has a greater effect than the decreased $J'_{Cu2+-Cr3+}$, thus resulting in a decrease in φ and moment canting and an increase in enhanced magnetization.

Finally, the nature of magnetism in CCO precludes the stabilization of alternative spin configurations. The magnetization in our films is too low for a Neél configuration. Long-range, coherent spiral ordering or uniform canting in one direction away from the field is also unlikely as PNR measurements find the absence of spin-flip scattering, thus indicating that there is no net [001] magnetization. Furthermore, despite lattice strains, our CCO films remain non-cubic making the Yafet-Kittel canted spin configuration likely as predicted by theoretical studies.[32]

In conclusion, we have successfully demonstrated the ability to induce greater spin alignment in canted, magnetically-frustrated CCO thin films via heteroepitaxy. By stabilizing a more cubic unit cell, we observe enhanced magnetization of CCO films that can be understood in terms of reducing the frustration of the magnetic lattice of CCO and modifying the strength of competing exchange interactions.

This work was supported by the National Science Foundation under Grants 0604277 and 1104401. The Advanced Light Source and the National Center for Electron Microscopy are supported by the Office of Basic Energy Sciences, Division of Materials Sciences and Engineering, of the U.S. Department of Energy under Contract No. DE-AC02-05CH11231. Portions of this research were carried out at the Stanford Synchrotron Radiation Lightsource, a national user facility operated by Stanford University on behalf of the U.S. Department of Energy, Office of Basic Energy Sciences. We would like to thank K. M. Yu, R. V. Chopdekar, J. S. Bettinger, V. V. Mehta, S. Anwar, and M. A. Mayer for assistance in data collection and discussion.

[1] A. P. Ramirez, in Handbook of Magnetic Materials, edited by K. J. H. Busch (Elsevier Science, Amsterdam, 2001).
[2] J. M. Hastings and L. M. Corliss, Phys. Rev. **126**, 556 (1962).
[3] N. Menyuk, K. Dwight, and A. Wold, J. Phys. **25**, 528 (1964).
[4] G. Shirane, D. E. Cox, and S. J. Pickart, J. Appl. Phys. **35**, 954 (1964).
[5] E. Prince, Acta Crystallogr. **10**, 554 (1957).
[6] K. Tomiyasu and I. Kagomiya, J. Phys. Soc. Jpn. **73**, 2539 (2004).
[7] T. A. Kaplan, Phys. Rev. **116**, 888 (1959).
[8] S. -H. Lee, H. Takagi, D. Louca, M. Matsuda, S. Ji, H. Ueda, Y. Ueda, T. Katsufuji, J.- H. Chung, S. Park, S. -W. Cheong, and C. Broholm, J. Phys. Soc. Jpn. **79**, 011004 (2010).
[9] Y. Yamasaki, S. Miyasaka, Y. Kaneko, J. - P. He, T. Arima, and Y. Tokura, Phys. Rev. Lett. **96**, 207204 (2006).
[10] C. Ederer and M. Komelj, Phys. Rev. B **76**, 064409 (2007).
[11] Y. Tokura and S. Seki, Adv. Mater. **22**, 1554 (2010).
[12] S. Bordács, D. Varjas, I. Kézsmárki, G. Mihály, L. Baldassarre, A. Abouelsayed, C. A. Kuntscher, K. Ohgushi, and Y. Tokura, Phys. Rev. Lett. **103**, 077205 (2009).
[13] G. Hu and Y. Suzuki, Phys. Rev. Lett. **89**, 276601 (2002).
[14] R. V. Chopdekar, B. B. Nelson-Cheeseman, M. Liberati, E. Arenholz, and Y. Suzuki, Phys. Rev. B **83**, 224426 (2011).
[15] J. M. Iwata, R. V. Chopdekar, B. B. Nelson-Cheeseman, F. J. Wong, and Y. Suzuki, (unpublished).
[16] M. Bibes, J. E. Villegas, A. Barthélémy, Adv. Phys. **60**, 5 (2011).
[17] M. G. Blamire, J. L. MacManus-Driscoll, N. D. Mathur, Z. H. Barber, Adv. Mater. **21**, 3827 (2009).
[18] A. Grutter, F. Wong, E. Arenholz, M. Liberati, A. Vailionis and Y. Suzuki, Appl. Phys. Lett. **96**, 082509 (2010).
[19] S. Miyahara and H. Ohnishi, J. Phys. Soc. Jpn. **11**, 1296 (1956).
[20] Y. Yafet and C. Kittel, Phys. Rev. **87**, 290 (1952).
[21] J. D. Dunitz and L. E. Orgel, J. Phys. Chem. Solids **3**, 20 (1957).
[22] Yu. S. Dedkov, A. S. Vinogradov, M. Fonin, C. König, D. V. Vyalikh, A. B. Preobrajenski, S. A. Krasnikov, E. Yu. Kleimenov, M. A. Nesterov, U. Rüdiger, S. L. Molodtsov, and G. Güntherodt, Phys. Rev. B **72**, 060401(R) (2005).
[23] M. Grioni, J. B. Goedkoop, R. Schoorl, F. M. F. de Groot, J. C. Fuggle, F. Schäfers, E. E. Koch, G. Rossi, J.-M. Esteva, and R. C. Karnatak, Phys. Rev. B **39**, 1541 (1989).
[24] B. B. Nelson-Cheeseman, R. V. Chopdekar, M. F. Toney, E. Arenholz, and Y. Suzuki, (to be published) J. Appl. Phys. (2012).
[25] J. M. Iwata, R. V. Chopdekar, F. J. Wong, B. B. Nelson-Cheeseman, E. Arenholz, and Y. Suzuki, J. Appl. Phys. **105**, 07A905 (2009).
[26] C. F. Majkrzak, Physica B **221**, 342 (1996).
[27] C. F. Majkrzak, K. V. O'Donovan, and N. Berk, in Neutron Scattering from Magnetic Materials, edited by T. Chatterji (Elsevier Science, New York, 2005).
[28] B. J. Kirby, D. Kan, A. Luykx, M. Murakami, D. Kundaliya, and I. Takeuchi, J. Appl. Phys. **105**, 07D917 (2009).
[29] V. F. Sears, in International Tables for Crystallography, edited by E. Prince, (Wiley, New York, 2006).
[30] In order to maintain beam polarization, our measurements were limited to fields below 700 mT. Hence reported PNR magnetization values are not obtained at saturation.
[31] J. B. Goodenough, in Magnetism and the Chemical Bond, (Krieger, New York, 1976).
[32] T. A. Kaplan, K. Dwight, D. Lyons, and N. Menyuk, J. Appl. Phys. **32**, S13 (1961).